The Journal of Immunology

The Endoplasmic Reticulum Adaptor Protein ERAdP Initiates NK Cell Activation via the Ubc13-Mediated NF-κB Pathway

Jun Chen, Lu Hao, Chong Li, Buqing Ye, Ying Du, Honglian Zhang, Bo Long, Pingping Zhu, Benyu Liu, Liuliu Yang, Peifeng Li, Yong Tian and Zusen Fan

J Immunol 2015; 194:1292-1303; Prepublished online 29 December 2014;
doi: 10.4049/jimmunol.1402593
http://www.jimmunol.org/content/194/3/1292

The Journal of Immunology is published twice each month by The American Association of Immunologists, Inc., 9650 Rockville Pike, Bethesda, MD 20814-3994.

Print ISSN: 0022-1767 Online ISSN: 1550-6606.

The Endoplasmic Reticulum Adaptor Protein ERAdP Initiates NK Cell Activation via the Ubc13-Mediated NF-κB Pathway

Jun Chen,*,†,[1] Lu Hao,*,†,[1] Chong Li,* Buqing Ye,* Ying Du,* Honglian Zhang,* Bo Long,‡ Pingping Zhu,* Benyu Liu,* Liuliu Yang,* Peifeng Li,§ Yong Tian,¶ and Zusen Fan*

NK cells play a pivotal role in innate immune responses against pathogenic infections. However, the underlying mechanisms driving defined NK functions remain largely elusive. In this study, we identified a novel endoplasmic reticulum (ER) membrane protein, ER adaptor protein (ERAdP), which is constitutively expressed in human and mouse NK cells. ERAdP is expressed at low levels in peripheral NK cells of hepatitis B virus–associated hepatocellular carcinoma patients. We show that ERAdP initiates NK cell activation through the NF-κB pathway. Notably, ERAdP interacts with ubiquitin-conjugating enzyme 13 (Ubc13) to potentiate its charging activity. Thus, ERAdP augments Ubc13-mediated NF-κB essential modulator ubiquitination to trigger the Ubc13-mediated NF-κB pathway, leading to NK cell activation. Finally, ERAdP transgenic mice display hyperactivated NK cells that are more resistant to pathogenic infections. Therefore, understanding the mechanism of ERAdP-mediated NK cell activation will provide strategies for treatment of infectious diseases. *The Journal of Immunology*, **2015, 194: 1292–1303.**

Natural killer cells, a major innate immune component, are defined as large granular lymphocytes, representing the third largest lymphoid cell population in mammals, and are critical in innate immune responses (1, 2). Cytokine secretion and direct killing are the two major effector functions of NK cells (3), acting as the first line of defense against pathogen infection and transformed tumors. NK cells can directly eradicate transformed or virus-infected cells very effectively (4–6). These functions are mediated by a series of germline-encoded receptors to deliver activating or inhibitory signals (7, 8). Besides their cytotoxic activity, NK cells robustly produce vast amounts of cytokines and chemokines (1, 3). IFN-γ produced by NK cells has been proven to exert critical roles in defense against pathogens as well as in immune regulation (9–11). However, the molecular mechanisms of NK cell activation have not yet been fully defined.

NF-κB was first reported to recognize the enhancer sequences in the gene encoding the Igκ L chain in B lymphoma (12). The NF-κB pathway plays a pivotal role in IFN-γ production of NK cells. After ligand binding or target cell adhesion, the NK cell surface receptors initiate an intracellular signaling cascade involving the activation of several major kinases and signaling complexes, ultimately leading to NF-κB activation. The ligand binding initially activates the receptor-associated Src kinases to phosphorylate Carma1. Carma1 phosphorylation promotes the Carma1/Bcl10/Malt1 (CBM) complex assembly, which recruits the ubiquitination machine E3 (TNFR-associated factor [TRAF]6)/E2 (ubiquitin-conjugating enzyme 13 [Ubc13]) complex and the NF-κB essential modulator (NEMO, also called IκB kinase [IKK]γ)/IKKα/β (IKK) complex (13). The ubiquitination of NEMO and phosphorylation of IKKα/β lead to full activation of the IKK complex and subsequent phosphorylation, which causes ubiquitination and degradation of its substrate IκBα (14), a cytoplasmic inhibitor of NF-κB. IκBα degradation releases the NF-κB and the free NF-κB is phosphorylated, which enters the nucleus to initiate target gene transcription.

The IKK complex is a central regulator of the NF-κB pathway, acting as a major target for ubiquitination and phosphorylation

*Chinese Academy of Sciences Key Laboratory of Infection and Immunity, Institute of Biophysics, Chinese Academy of Sciences, Beijing 100101, China; †University of Chinese Academy of Sciences, Beijing 100049, China; ‡Central Research Laboratory, Peking Union Medical College Hospital, Chinese Academy of Medical Sciences and Peking Union Medical College, Beijing 100730, China; §State Key Laboratory of Biomembrane and Membrane Biotechnology, Institute of Zoology, Chinese Academy of Sciences, Beijing100101, China; and ¶Beijing Noncoding RNA Laboratory, Institute of Biophysics, Chinese Academy of Sciences, Beijing 100101, China

[1]J.C. and L.H. contributed equally to this work.

Received for publication October 14, 2014. Accepted for publication November 29, 2014.

This work was supported by National Natural Science Foundation of China Grants 81330047 and 31170837, by Grants 2015CB553705 and 2010CB911902 from the 973 Program of the Ministry of Science and Technology of China, and by the Strategic Priority Research Programs of the Chinese Academy of Sciences (Grant XDA01010407).

J.C. and L.H. designed and performed experiments, analyzed data, and wrote the manuscript; C.L., Y.D., P.Z., B. Liu, and L.Y. performed some experiments; B.Y. and H.Z. analyzed data; B. Long and P.L. generated Tg mice; Y.T. generated knockout mice; and Z.F. initiated the study and organized, designed, and wrote the paper.

The microarray data presented in this article have been submitted to the National Center for Biotechnology Information's Gene Expression Omnibus database (http://www.ncbi.nlm.nih.gov/geo/query/acc.cgi?acc=GSE63214) under accession number GSE63214. The sequences presented in this article have been submitted to GenBank (http://www/ncbi.nlm.nih.gov/genbank/) under accession number FJ516381.1.

Address correspondence and reprint requests to Dr. Zusen Fan, Dr. Yong Tian, or Dr. Peifeng Li, Chinese Academy of Sciences Key Laboratory of Infection and Immunity, Institute of Biophysics, Chinese Academy of Sciences, Beijing 100101, China (Z.F.), Beijing Noncoding RNA Laboratory, Institute of Biophysics, Chinese Academy of Sciences, Beijing 100101, China (Y.T.), or State Key Laboratory of Biomembrane and Membrane Biotechnology, Institute of Zoology, Chinese Academy of Sciences, Beijing 100101, China (P.L.). E-mail addresses: fanz@moon.ibp.ac.cn (Z.F.), ytian@ibp.ac.cn (Y.T.), or peifli@ioz.ac.cn (P.L.)

The online version of this article contains supplemental material.

Abbreviations used in this article: BD, binding domain; CARD, caspase recruitment domain; CBM, Carma1/Bcl10/Malt1; Ctrl, control; ER, endoplasmic reticulum; ERAdP, ER adaptor protein; HBV, hepatitis B virus; HCC, hepatocellular carcinoma; IKK, IκB kinase; IKK complex, IκB kinase γ/IκB kinase α/β complex; IONO, ionomycin; NEMO, NF-κB essential modulator; shRNA, short hairpin RNA; Tg, transgenic; TRAF, TNFR-associated factor; Ubc13, ubiquitin-conjugating enzyme 13.

www.jimmunol.org/cgi/doi/10.4049/jimmunol.1402593

regulation. TRAF6 is the E3 ligase of NEMO and mediates its K63-linked ubiquitination, which transduces activating signals to initiate activation of the IKK complex (15, 16). Ubc13 has been defined as the E2 ligase of this process and is an essential component of the ubiquitination machinery for NF-κB activation (15, 17, 18). Ubc13 deficiency in thymocytes leads to abolished ubiquitination of NEMO and phosphorylation of TGF-β–activated kinase 1 (19). Ubc13 forms a complex with Uev1a (human homolog of yeast Mms2) as an E2 ligase (20, 21). In the E2/E3 complex, TRAF6 selects substrates and Ubc13 ingeniously determines the linkage specificity and the length of polyubiquitin chains (18, 22–24). Ubc13 was reported to be important for TCR signaling of T lymphocytes (19). However, it is unclear whether and how Ubc13 is involved in NK cell activation. In this study, we identified a novel endoplasmic reticulum (ER) membrane protein, which we call ER adaptor protein (ERAdP). ERAdP is constitutively expressed in NK cells. ERAdP interacts with Ubc13 to activate the Ubc13-mediated NF-κB pathway, leading to NK cell activation.

Materials and Methods

Cell culture

293T and 293A cells were grown in DMEM (Life Technologies) with 10% FBS (Life Technologies), 50 μM 2-ME, 100 U/ml penicillin, and 100 mg/ml streptomycin. Transient transfection was performed using Neofectamine (Qiagen) following the manufacturer's protocol. NKL and primary NK cells were cultured in RPMI 1640 medium (Life Technologies) with 500 U/ml IL-2 and 10% FBS.

Abs and reagents

We used the following Abs: anti-EEA1, anti-calreticulin, and anti–COX IV Abs (Abcam); anti–enhanced GFP and anti–CD3-FITC Abs (Tianjin Sungenebiotech); anti–β-actin, anti-Flag, and anti-His Abs (Sigma-Aldrich); anti–IFN-γ-PE, anti–NK1.1-allophycocyanin, anti–DX5-FITC, anti–TNF-α-FITC, and anti–CD56-allophycocyanin Abs (eBioscience); anti–phospho-IκBα, anti-IKKβ, anti–phospho-p65, anti–phospho-ERK1/2, anti-ERK1/2, anti–histone 3, anti–phospho-PI3K-p85, anti–PI3K-p85, and anti–phospho-IKKα/β Abs (Cell Signaling Technology); anti-IκBα, anti-NEMO, anti-TRAF6, anti-Carma1, anti-Malt1, and anti-Bcl10 Abs (Santa Cruz Biotechnology); anti-Ubc13 Ab (Invitogen); and anti-ubiquitin Ab (Enzo Life Sciences). All secondary Abs were from Zhongshan Jinqiao Company. Polyclonal anti-ERAdP Ab was generated from keyhole limpet hemocyanin–linked ERAdP peptides by our own laboratory. PMA/ionomycin (IONO), NF-κB inhibitor (BAY 11-7085), PI3K inhibitor (wortmannin), polylysine, and cycloheximide were from Sigma-Aldrich; brefeldin A was from eBioscience. The CD2 promotor–driven transgenic (Tg) vector was a gift from Dr. André Veillette (Institut de Recherches Cliniques de Montréal, Montreal, QC, Canada). The Ubc13 inhibitor (compound NSC697923) was a gift from Dr. Jiyong Zhao (University of Rochester Medical Center, Rochester, NY) and the National Cancer Institute Developmental Therapeutic Program.

Gene expression profiling through microarray

Total RNA was extracted from peripheral NK cells of hepatitis B virus (HBV)–associated hepatocellular carcinoma (HCC) patients and healthy donors using standard RNA extraction protocol, followed by DNase incubation to remove nuclear DNA. The quality of RNA was monitored by NanoDrop, and the integrity of RNA was tested by agarose gel electrophoresis. Total RNA was subjected to labeling and array hybridization using a Phalanx Human OneArray expression array according to the manufacturer's instructions (Phalanx Biotech Group). The hybridized array was scanned using the GenePix 4100 microarray scanner (Molecular Devices), followed by grid alignment and expression analysis using the OneArray software. The microarray data have been deposited in National Center for Biotechnology Information Gene Expression Omnibus database (http://www.ncbi.nlm.nih.gov/geo/query/acc.cgi?acc=GSE63214) under accession number GSE63214. The collection of human blood samples was approved by the Medical Research Ethics Committee at the Institute of Biophysics, Chinese Academy of Sciences.

NK cell transfection

NKL cells were nucleofected as reported (25). Briefly, a total of 2×10^6 cells were resuspended in 100 μl Amaxa kit V, mixed with 300 pmol short hairpin RNA (shRNA), and immediately transfected with program O-017 in the Amaxa Nucleofector system. Cells were incubated for at least 36 h and then stimulated with PMA/IONO to detect IFN-γ expression by flow cytometry or ELISA. For stably transfected NKL cells, NKL cells were transfected with replication defective virus packed by lentivirus-based vector pSin, gag-pol, and envelope plasmids and selected by 0.25 μM puromycin to establish stably transfected cell lines.

Yeast two-hybrid screening

Yeast two-hybrid screening was performed using a Matchmaker gold yeast two-hybrid system (Clontech/TaKaRa) under the guidelines provided by the manufacturer. Briefly, ERAdP was subcloned into the pGBKT7 vector with DNA binding domain (BD) (BD-ERAdP). Yeast AH109 cells were transfected with BD-ERAdP and plasmids containing a human spleen cDNA library (Clontech/TaKaRa) and then plated on SD medium lacking adenine, histidine, tryptophan, and leucine. Selected clones were isolated and identified by DNA sequencing. Recovery of the plasmids and X-α-gal assay were carried out as described (26). AD-p53 and BD–large T Ag were cotransfected as a positive control (Ctrl).

Coimmunoprecipitation and immunoblotting

Coimmunoprecipitation and immunoblotting were done as previously described (27). Six-well dishes of 293T cells were grown overnight and each dish was transfected with a total of 1–4 μg of the indicated plasmids using Neofectamine (Qiagen). After 48 h, cells were lysed in 600 μl cold lysis buffer (50 mM Tris-HCl [pH 7.5], 150 mM NaCl, 2 mM EDTA, and 0.25% Nonidet P-40 supplemented with protease and phosphatase inhibitor cocktails). Cell lysates were subjected to immunoprecipitation with the indicated Abs. Immunoprecipitations were incubated at 4˚C overnight. Immunoprecipitates were washed three times with lysis buffer. The beads were then boiled in 25 μl SDS sample loading buffer and subjected to Western blotting.

NKL cell fraction isolation

Mitochondrial and ER membrane fractions were purified on discontinuous sucrose gradients from NKL cells as previously described (28). Briefly, cells in fraction isolation buffer (Tris-HCl [10 mM, pH 7.4], mannitol (0.27 M), 0.1 mM EDTA, protease, and phosphatase inhibitor cocktails) were subjected to homogenization. After centrifugation at 700 × *g* at 4˚C for 10 min, the supernatant (postnuclear solution) was saved. The postnuclear solution was centrifugated at 15,000 × *g* for 10 min. The pellet was resuspended in fraction isolation buffer, layered on discontinuous sucrose gradients (1.0 and 1.5 M sucrose in 10 mM Tris-HCl [pH 7.5]) and centrifuged at 60,000 × *g* for 30 min. The mitochondrial and endosomal fractions were collected and pelleted by centrifugation at 17,000 × *g* for 25 min. To isolate ER fractions, postmitochondrial supernatants were layered on discontinuous sucrose gradients (1.3, 1.5, and 2.0 M sucrose in 10 mM Tris-HCl [pH 7.5]) and centrifuged at 87,000 × *g* for 100 min. The membrane enriched at the interface between the supernatant and the 1.3 M sucrose was the ER fraction. It was collected and pelleted by centrifugation at 87,000 × *g* for 45 min and the pellets were resuspended in PBS and prepared for Western blot analysis.

In vitro ubiquitination reconstitution assay

Assays were performed in ubiquitination reaction buffer (50 mM Tris-HCl [pH 8.0], 5 mM $MgCl_2$, 2 mM ATP). His-Ube1 (0.0125 mM), 0.4 mM E2 (His-UBC13/Uev1a), His-ubiquitin (40 mM), 0.2 mM recombinant E3 (Flag-TRAF6), and 0.2 mM Flag-NEMO were incubated with or without recombinant Flag-ERAdP. Reaction mixtures were incubated at 37˚C for 2 h. Reactions were stopped by SDS loading buffer and samples were immunoprecipitated by anti-NEMO Ab and immunoblotted with anti-His Ab.

Ubc13 charging activity assay

Charging reaction was performed in ubiquitin charging reaction buffer (50 mM Tris-HCl [pH 8.0], 5 mM $MgCl_2$, and 1 mM ATP). Reaction buffer containing recombinant His-Ube1 (0.04 mM), His-Ubc13 (2 mM), and His-ubiquitin (5 mM), with or without recombinant Flag-ERAdP protein (5 mM), was assembled and incubated at 37˚C for 40 min. Samples were immunoblotted with anti-Ubc13 Ab.

Generation of Flag-ERAdP Tg mice

Mouse experiments were approved by the Institutional Animal Care and Use Committee at the Institute of Biophysics, Chinese Academy of Sciences. Eggs from hormonally superovulated female C57BL/6 mice were microinjected with purified linear CD2-Flag-ERAdP expression vector. Injected fertilized eggs were transplanted into the oviduct of pseudopregnant

F_1 hybrids of C57BL/6 mice. Then, founder mice were identified by PCR analysis of genomic DNA from the tails of Tg mice offspring. Founder mice were crossed with wild-type C57BL/6 mice to generate the Tg and littermate Ctrl mice used for all experiments.

Listeria monocytogenes *infection*

For survival curve analysis, Tg and Ctrl mice were i.p. injected with 2×10^6 *L. monocytogenes* without or with depletion of NK cells by anti-Asialo GM1 mAb. Death rates were observed daily until day10. For sublethal dose infections, mice were inoculated i.p. with 3×10^5 *L. monocytogenes*. Bacteria in the spleen and liver were measured on day 3 postinfection. Spleen and liver were homogenized with PBS and the supernatants were streaked on plates at various titrations. Total colonies of liver or spleen were calculated after incubation at 37˚C overnight. IFN-γ detection by flow cytometry was performed at 24 h after sublethal dose infection, whereas IFN-γ was detected by ELISA in Tg and Ctrl mice on day 3 postinfection.

Statistical analysis

A Student *t* test was used for statistical analysis with SigmaPlot software.

Results

ERAdP is a conserved ER membrane protein and is constitutively expressed in NK cells

We previously demonstrated that chronic HBV carriers and HBV-associated HCC patients display low rates of granzyme H^+ NK cells in the periphery and in livers (5). We then carried out DNA microarray analysis of peripheral NK cells from HBV-associated HCC patients versus healthy donors. We analyzed differentially expressed genes in HBV-associated HCC patients. Among the lowly expressed differential genes, we focused on a novel gene

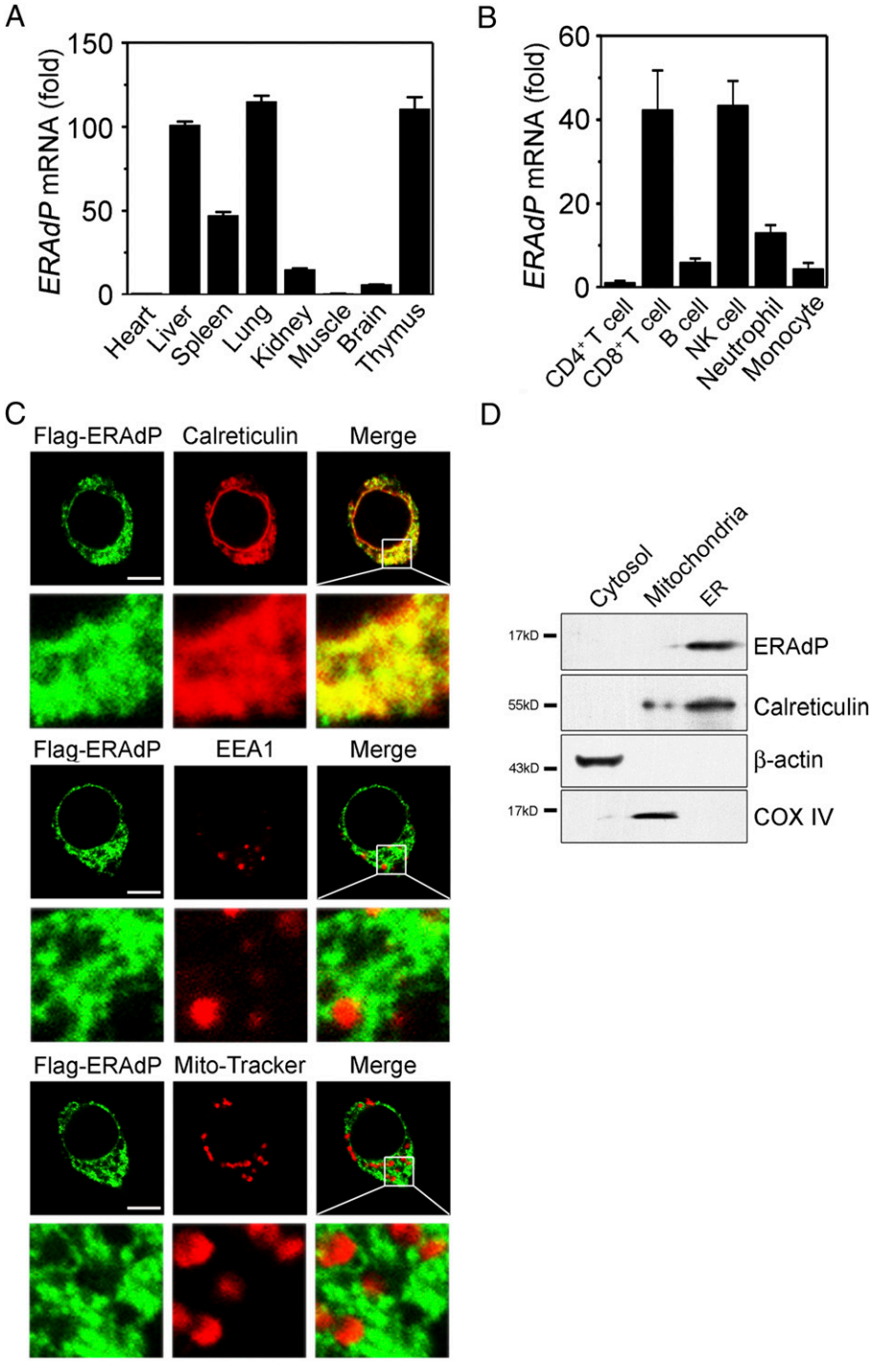

FIGURE 1. ERAdP is an ER protein that is constitutively expressed in NK cells. (**A**) ERAdP is constitutively expressed in immune organs. Total RNAs were extracted from murine tissues and analyzed by quantitative RT-PCR. Expression was normalized to GAPDH and is presented as fold change relative to *ERAdP* expression in heart. Graphs are shown as means ± SD. (**B**) *ERAdP* is highly expressed in NK cells and $CD8^+$ T cells. Mouse blood cell types were isolated by a FACS sorter and their RNAs were extracted for quantitative RT-PCR assays. *ERAdP* mRNA expression levels of each cell type were normalized to *GAPDH* from the same cell type. The value of $CD4^+$ T cells was set as 1. Fold change was relative to the *ERAdP* expression in $CD4^+$ T cells. (**C**) ERAdP is localized on ER. Flag-ERAdP plasmids were transfected into NKL cells for 24 h and were analyzed by immunofluorescence staining. Calreticulin staining red stands for ER, EEA1 for early endosomes, and MitoTracker staining red for mitochondria (*middle panels*). Flag-ERAdP staining green (*left panels*) and merged images (*right panels*). Original magnification ×400. Scale bars, 5 μm. (**D**) NKL cell lysates were fractionated by discontinuous sucrose gradient ultracentrifugation. Purified fractions were probed by immunoblotting.

variant of TMEM188. We cloned the full length of the new variant TMEM188, called ERAdP, which was submitted to GenBank (FJ516381.1). ERAdP was highly expressed in peripheral NK cells in healthy donors (Supplemental Fig. 1A) but was downregulated in HBV-associated HCC patients, as was the case with immune effector molecules such as perforin and granzyme H (5). These data suggest that ERAdP may positively regulate NK cell activation.

ERAdP contains 125 aa residues and is highly conserved in vertebrates. It shares the same protein sequence as its mouse ortholog, ~97.6% sequence identity with the frog, and even 53% identity with the fly (Supplemental Fig. 1A). *ERAdP* mRNA was ubiquitously transcribed in a variety of mouse tissues, but it was highly expressed in immune-related organs (Fig. 1A). Notably, *ERAdP* mRNA was highly expressed in NK and $CD8^+$ T cells in wild-type mice (Fig. 1B). In contrast, it was lowly expressed in other immune cells, including $CD4^+$ T cells, B cells, monocytes, and neutrophils. Similar results were also observed in human counterpart cells (data not shown).

Because ERAdP has two putative transmembrane domains (Supplemental Fig. 1B), we next examined its exact cellular localization. We overexpressed ERAdP in human NKL cells with a Flag tag and observed that ERAdP was localized on the ER membrane, but not on the mitochondria or early endosomes (Fig. 1C). These observations were further verified by organelle fractionation analysis of NKL cells (Fig. 1D). Additionally, to further determine whether the two transmembrane domains of ERAdP were essential for the ER location, we overexpressed ERAdP in human 293A cells with an enhanced GFP tag. ERAdP residing in the ER was also displayed in 293A cells (Supplemental Fig. 1C). Importantly, deletion of each transmembrane domain of ERAdP abolished its ER residence (Supplemental Fig. 1D), suggesting that both of the transmembrane domains were essential for ER

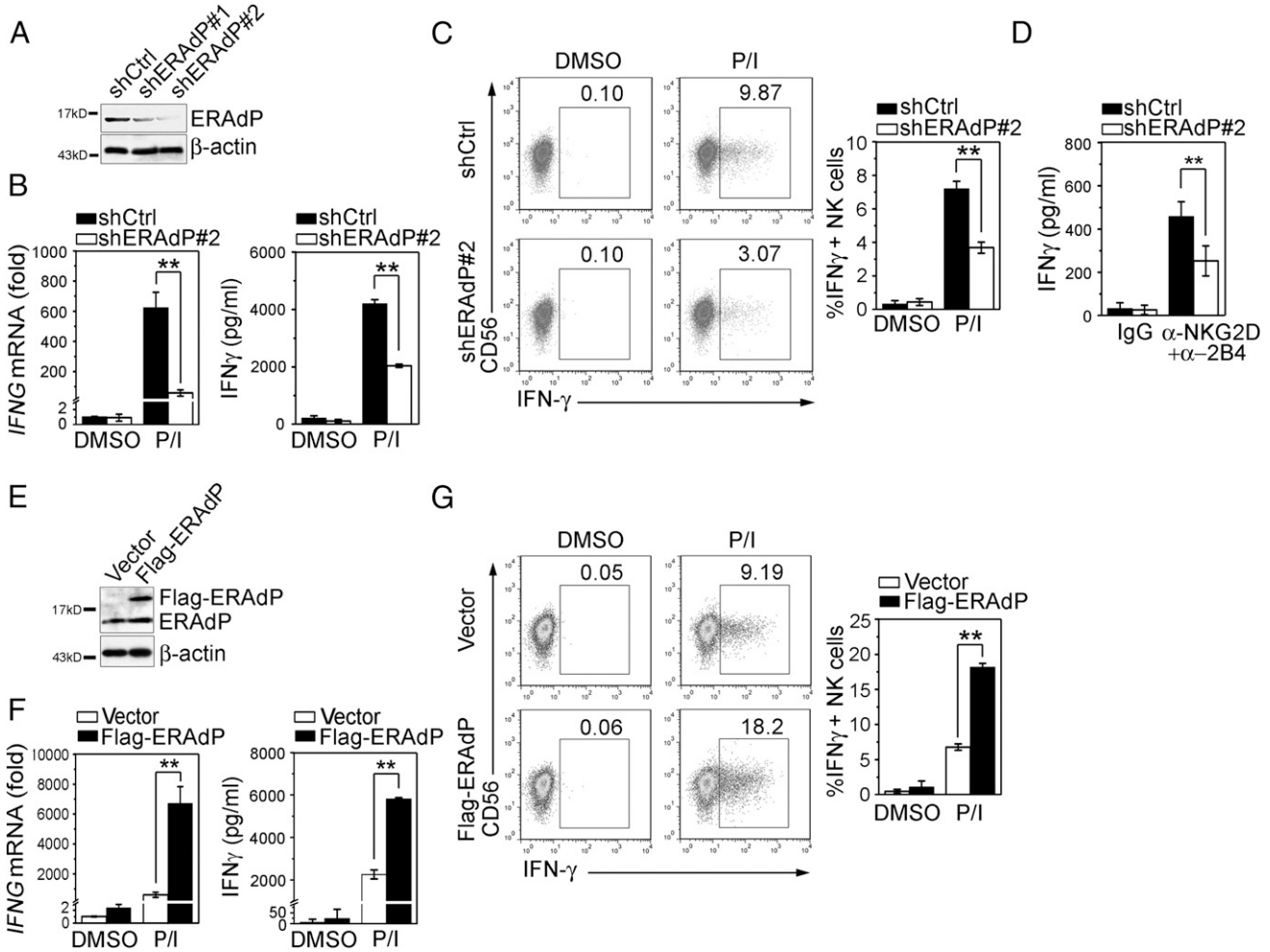

FIGURE 2. ERAdP potentiates NK cell activation to induce IFN-γ production. (**A**) ERAdP was silenced by shERAdP. ERAdP stably depleted NKL cell lines were established by puromycin selection. (**B**) ERAdP-silenced NKL cells dramatically decline IFN-γ secretion. After 6 h of PMA (50 ng/ml)/IONO (1 μg/ml) treatment, *IFNG* mRNA was detected by quantitative RT-PCR; results are relative to those of scramble Ctrl cells (*left panel*). Protein levels of IFN-γ in NK cell supernatants were analyzed by ELISA assays after 24 h with PMA/IONO stimulation (*right panel*). (**C**) IFN-γ expression was verified by flow cytometry. ERAdP-silencing NKL cells were treated with PMA/IONO for 6 h (*left panel*), followed by brefeldin A (10 μg/ml) treatment for intracellular IFN-γ staining. Data from three independent experiments are shown as means ± SD (*right panel*). (**D**) ERAdP silencing also decreases IFN-γ generation by crosslinking with NK cell receptors. Anti-NKG2D plus anti-2B4 Abs were precoated on 96-well plates at 4°C overnight. Silencing ERAdP NKL cells and scramble Ctrl cells were cultured in precoated wells for 24 h. Supernatants were collected for IFN-γ detection by ELISA assays. (**E**) ERAdP stably overexpressing NKL cell lines were generated by puromycin selection. (**F**) ERAdP overexpressing NKL cells remarkably increases IFN-γ production. Detection of mRNA (*left panel*) and protein levels (*right panel*) of IFN-γ in ERAdP-overexpressing NKL cells was as above. (**G**) Flow cytometry analysis of IFN-γ expression in ERAdP-overexpressing NKL cells stimulated with PMA/IONO for 6 h (*left panel*). Statistical data from three independent FACS experiments are shown as means ± SD (*right panel*). $^{**}p < 0.01$.

localization of ERAdP. Taken together, ERAdP is a highly conserved ER membrane protein, which is constitutively expressed in NK cells.

ERAdP initiates IFN-γ production of NK cells

To determine functions of ERAdP in NK cells, we knocked down ERAdP expression in human NKL cells and established stable ERAdP-silencing cell lines (Fig. 2A). PMA and IONO can directly activate protein kinase C kinases to induce NF-κB activation in lymphocytes. After PMA/IONO treatment, ERAdP-silenced NKL cells dramatically declined IFN-γ generation both in mRNA and protein levels compared with those of scramble shRNA–treated cells (Fig. 2B). These phenomena were confirmed by flow cytometry (Fig. 2C). To exclude off-targeting effects of shRNA-mediated gene silencing, we designed two independent shRNA sequences against ERAdP mRNA and both of them effectively silenced ERAdP and IFN-γ expression in NKL cells (data not shown). Additionally, we still checked TNF-α and GM-CSF production after ERAdP depletion. We noticed that ERAdP silencing also reduced the production of TNF-α and GM-CSF (data not shown). NK cells use various receptors to recognize their corresponding ligands for NK cell activation. Synergistic coactivation by NKG2D and 2B4 receptors was reported to activate NK cells and induce IFN-γ production (25). We found that ERAdP-silenced NKL cells secreted much less IFN-γ by crosslinking with NKG2D and 2B4 receptors (Fig. 2D). These data suggest that ERAdP facilitates IFN-γ secretion of NK cells in both PMA/IONO stimulation and physiological crosslinking of the activation receptors.

We next transfected NKL cells with lentivirus encoding ERAdP and obtained NKL cell lines stably overexpressing Flag-ERAdP (Fig. 2E). With PMA/IONO treatment, ERAdP overexpression remarkably increased IFN-γ expression compared with those of empty vector–transfected Ctrl cells (Fig. 2F, 2G). Additionally, ERAdP overexpression also increased the generation of TNF-α and GM-CSF (data not shown). Similar results were obtained by crosslinking NKG2D and 2B4 receptors (data not shown). In summary, ERAdP can induce NK cell activation to promote cytokine secretion.

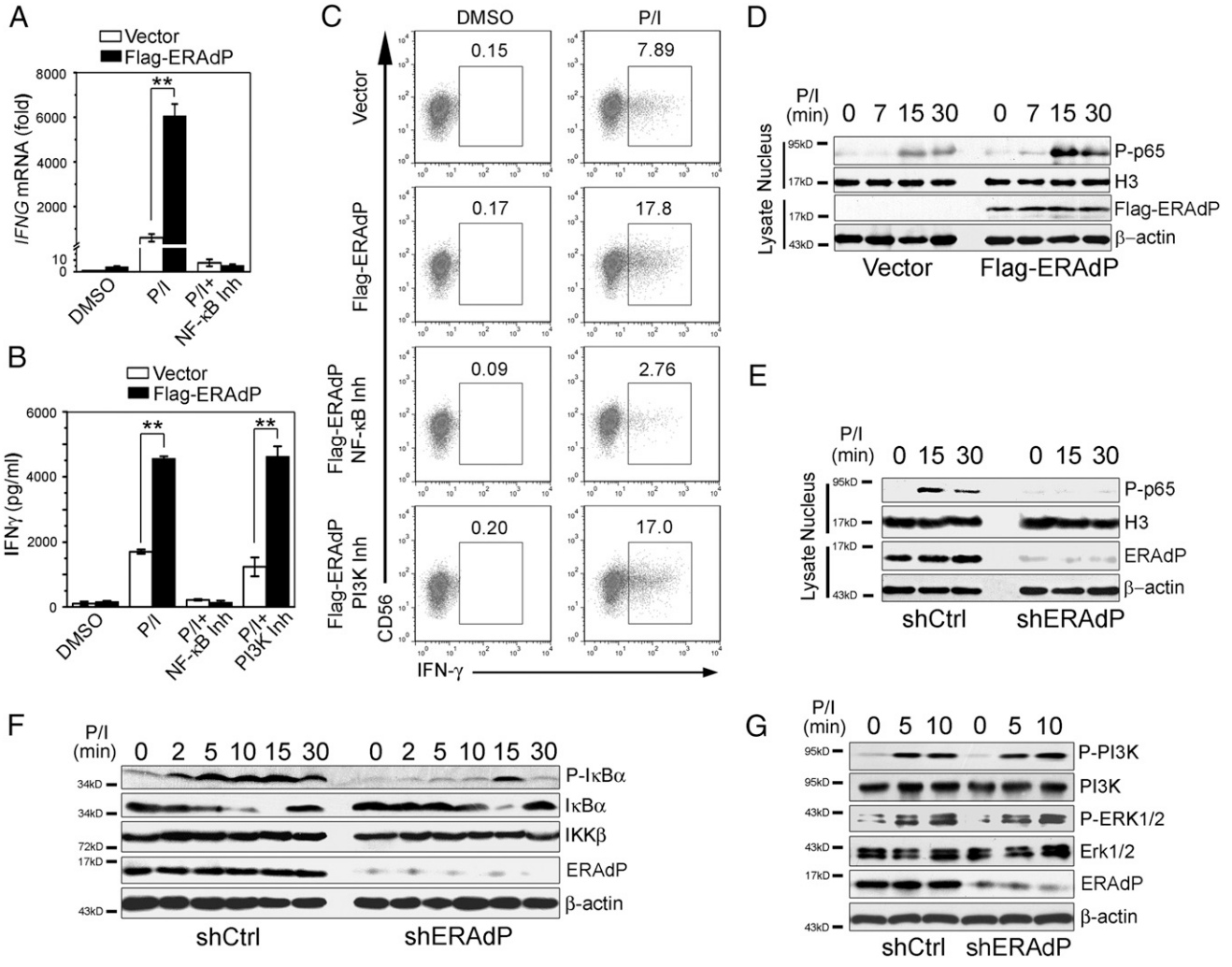

FIGURE 3. ERAdP mediates NK cell activation via the NF-κB pathway. (**A**–**C**) The NF-κB pathway but not the PI3K pathway is required for ERAdP-mediated IFN-γ secretion. Flag-ERAdP–overexpressing NKL cells or Ctrl cells were pretreated with the NF-κB inhibitor (BAY11-7085) or the PI3K inhibitor (wortmannin) for 2 h, followed by PMA/IONO treatment for 6 (A and C) or 24 h (B). Samples were analyzed for IFN-γ. PMA/IONO-treated cells were used as experimental Ctrls. (**D** and **E**) ERAdP promotes p65 activation. ERAdP-overexpressing (D) or depleted (E) NKL cells were stimulated with PMA/IONO for the indicated times. Nuclear and cytosolic portions were separated and probed with the indicated Abs. (**F**) ERAdP silencing dramatically promotes degradation of IκBα. ERAdP-silencing NKL cells and Ctrl cells were stimulated with PMA/IONO for the indicated times followed by immunoblotting. β-Actin served as a loading Ctrl. (**G**) ERAdP silencing does not affect the PI3K and ERK pathways. NKL cells were stimulated with PMA/IONO for the indicated times followed by immunoblotting. Data are representative of at least three independent experiments. $^{**}p < 0.01$.

ERAdP-mediated IFN-γ production requires the NF-κB activation pathway

To examine whether ERAdP regulates the NF-κB pathway, we pre-incubated NKL cells with the NF-κB inhibitor BAY11-7085 before PMA/IONO stimulation. Interestingly, we found that the NF-κB inhibitor completely blocked ERAdP-mediated IFN-γ production (Fig. 3A–C). However, the PI3K inhibitor wortmannin had no such activity (Fig. 3B, 3C). Consequently, the phosphorylation of p65 occurred more rapidly at early time points in cells overexpressing ERAdP (Fig. 3D). However, ERAdP-silenced NK cells almost blocked the phosphorylation of p65 (Fig. 3E), as well as the phosphorylation of IκBα (Fig. 3F). Additionally, ERAdP silencing did not affect PI3K or ERK signaling pathways (Fig. 3G). These data indicate that ERAdP specifically facilitates the NF-κB activation pathway.

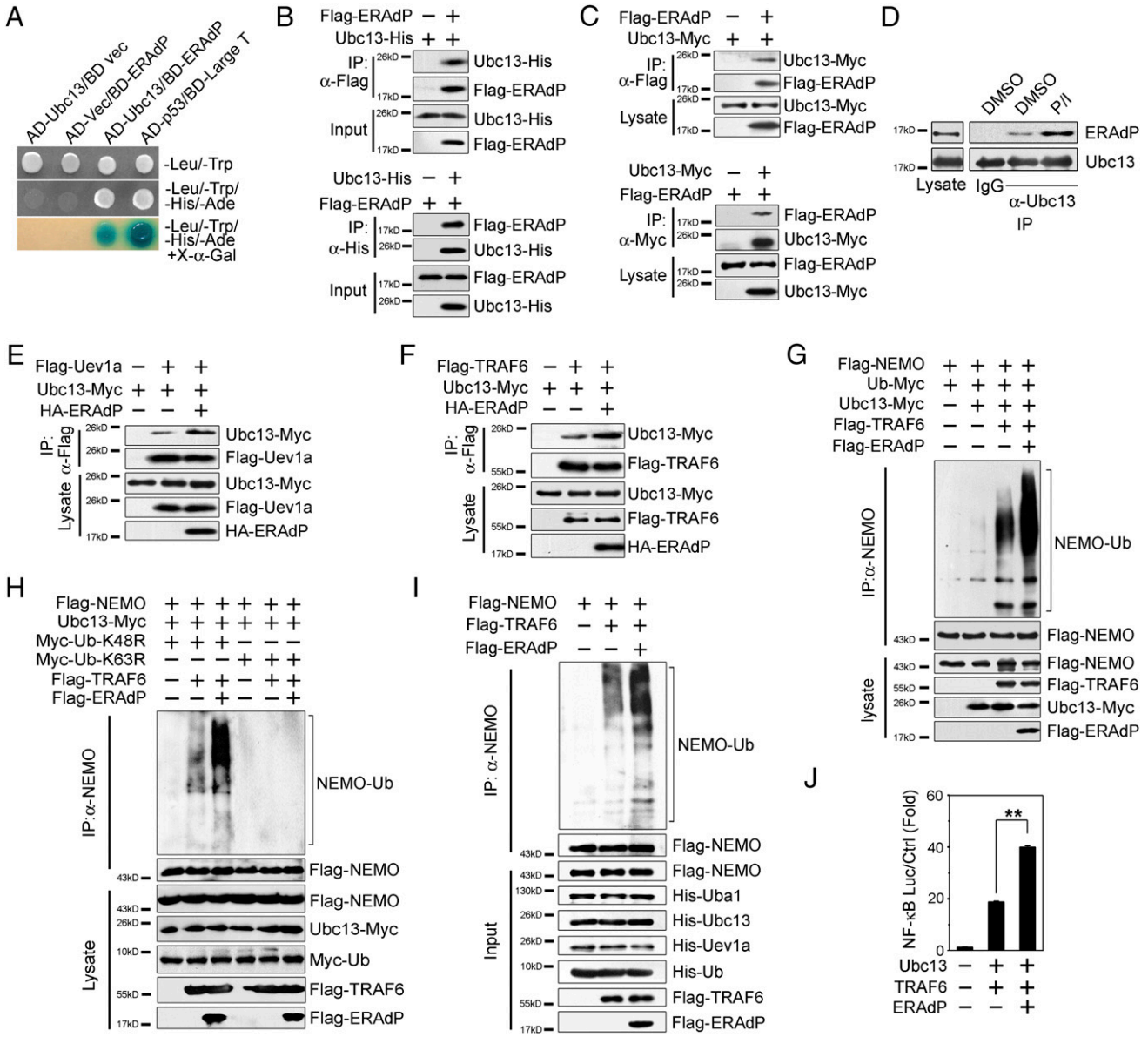

FIGURE 4. ERAdP associates with Ubc13 to promote NEMO ubiquitination. (**A**) Ubc13 is an interacting protein of ERAdP via yeast two-hybrid screening. Yeast AH109 strain was cotransfected with Gal4 DNA binding domain (BD) fused with ERAdP and Gal4 activating domain (AD) fused with Ubc13. p53 and large T Ag was used as a positive Ctrl. (**B**) ERAdP directly interacts with Ubc13. Recombinant Flag-ERAdP and Ubc13-His were incubated at 4˚C for 4 h and precipitated with anti-Flag or anti-His Abs, followed by immunoblotting. (**C**) The association of ERAdP with Ubc13 was confirmed by coimmunoprecipitation. 293T cells were transfected with Flag-ERAdP and Ubc13-Myc plasmids for 48 h. Cells were harvested and lysates were precipitated with anti-Flag or anti-Myc Abs. (**D**) The association of ERAdP with Ubc13 appears in NK cells. NKL cells were stimulated with PMA/IONO for 15 min and lysates were immunoprecipitated with anti-Ubc13 Ab. (**E** and **F**) ERAdP augments the interaction of Ubc13 with Uev1a and Ubc13 with TRAF6. 293T cells were transfected with the indicated plasmids and detected by immunoprecipitation assays. (**G** and **H**) ERAdP overexpression enhances K63-linked ubiquitination of NEMO. Flag-NEMO, Ub-Myc, Ub-K48R-Myc, Ub-K63R-Myc, Flag-TRAF6, Ubc13-Myc, and Flag-ERAdP were transfected into 293T cells for 48 h. Cell lysates were immunoprecipitated with anti-NEMO Ab and probed with anti-Myc Ab. (**I**) ERAdP-enhanced ubiquitination of NEMO was verified by an in vitro ubiquitination reconstitution assay. In vitro ubiquitination assays were performed by incubating the indicated purified recombinant proteins and ATP in the ubquitination reaction buffer at 37˚C for 2 h. Samples were immunoprecipitated by anti-NEMO Ab and immunoblotted with anti-His Ab. (**J**) ERAdP promotes NF-κB activation through a luciferase reporter assay. Flag-ERAdP, Ubc13-Myc, Flag-TRAF6, and luciferase reporter vectors were transfected into 293T cells for 48 h. Lysates were harvested and NF-κB activation was determined by luciferase reporter assays. Data are representative of three independent experiments. $^{**}p < 0.01$.

ERAdP activates the NF-κB pathway via regulation of NEMO ubiquitination

Activation of the NF-κB pathway encompasses several key steps, including the CBM complex assembly, phosphorylation of IKKα/β, and ubiquitination of NEMO (also called IKKγ). Intriguingly, Carma1 assembled the same amount of Bcl10/Malt1 subcomplex in ERAdP-silenced NKL cells as did that of scramble-treated Ctrl NKL cells (Supplemental Fig. 2A). Furthermore, phosphorylation of IKKα/β was comparable in ERAdP-silenced compared with scramble-treated Ctrl NKL cells (Supplemental Fig. 2B). However, ERAdP silencing significantly declined ubiquitination of NEMO compared with scramble-treated Ctrl NKL cells (Supplemental Fig. 2C). These results suggest that ERAdP activates the NF-κB pathway via modulation of ubiquitination of NEMO.

ERAdP interacts with Ubc13 to mediate K63-linked ubiquitination of NEMO

To determine the molecular mechanism of ERAdP-mediated NF-κB activation pathway, we screened a human spleen cDNA library

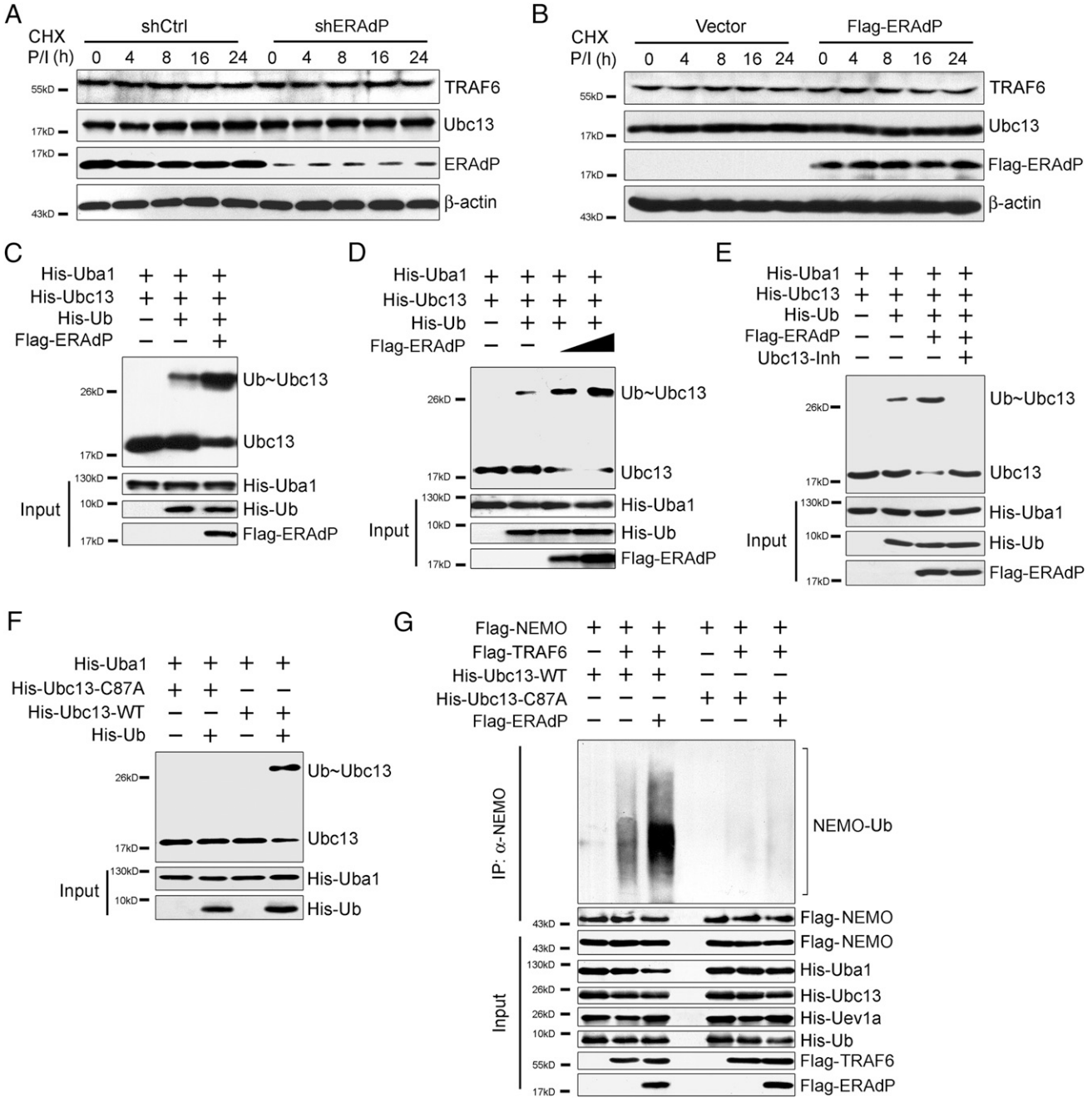

FIGURE 5. ERAdP potentiates the charging activity of Ubc13. (**A** and **B**) ERAdP does not affect the stability of Ubc13 and TRAF6. After preincubation of cycloheximide (CHX) (20 μg/ml) for 2 h, NKL cells were stimulated with PMA/IONO for the indicated times, followed by immunoblotting. (**C** and **D**) ERAdP enhances the charging activity of Ubc13. Recombinant His-Uba1, His-Ubc13, and His-Ub were incubated in charging buffer at 37˚C for 40 min, with or without Flag-ERAdP (C) and with different doses of Flag-ERAdP (D). Ubc13 charging activity was analyzed by immunoblotting with anti-Ubc13 Ab. (**E**) The Ubc13 inhibitor blocks the ERAdP-enhanced charging activity of Ubc13. The Ubc13 inhibitor NSC697923 (2 μM) was pretreated for 1 h prior to incubation with other components. (**F**) The Ubc13-C87A mutant blocks the charging activity of Ubc13. Ubc13-WT or inactive mutant Ubc13-C87A was incubated with E1 (His-Ube1), His-Ub, and ATP in charging buffer at 37˚C for 40 min. (**G**) The Ubc13-C87A mutant also blocks the ubiquitination of NEMO. Ubc13-WT or Ubc13-C87A was incubated with the in vitro ubiquitination system components as described in Fig. 4I.

to identify ERAdP's interacting protein by using a yeast two-hybrid assay. Ubc13 was identified as an interacting protein of ERAdP (Fig. 4A). Ubc13 was reported to catalyze K63-linked polyubiquitin chains for many important proteins as an E2 ligase (16). Deletion of Ubc13 in T lymphocytes causes defective ubiquitination of NEMO and abolishes activation of NF-κB signaling (19). Thus, we proposed that ERAdP may activate NK cells through the Ubc13-mediated NF-κB activation pathway. We found that recombinant Flag-ERAdP and Ubc13-His can directly interact with each other (Fig. 4B). Moreover, their interaction was confirmed by coimmunoprecipitation in 293T cells (Fig. 4C) and NKL cells (Fig. 4D). With PMA/IONO stimulation, the association of endogenous ERAdP and Ubc13 was dramatically augmented in NKL cells (Fig. 4D). These data suggest that NK cell activation can enhance the association of ERAdP and Ubc13.

Ubc13 binds Uev1a to form the E2/E3 complex with TRAF6. Ubc13 and TRAF6 were reported to mediate ubiquitination of NEMO (16). We proposed that ERAdP may promote NEMO ubiquitination via the assistance of Ubc13. Surprisingly, we found that ERAdP markedly strengthened the association among Ubc13 with Uev1a and TRAF6 (Fig. 4E, 4F), suggesting that ERAdP helped the assembly of the Ubc13 ligase complex. Importantly, ERAdP significantly facilitated TRAF6- and Ubc13-mediated ubiquitination of NEMO (Fig. 4G). Additionally, ERAdP specifically enhanced K63-linked ubiquitination of NEMO, but not K48-linked ubiquitination (Fig. 4H).

To verify these observations, we established an in vitro ubiquitination reconstitution assay. Incubation of all the essential recombinant components catalyzed the ubiquitination of NEMO (Fig. 4I). Actually, ERAdP indeed promoted NEMO ubiquitination (Fig. 4I). More importantly, ERAdP could enhance Ubc13-mediated NF-κB reporter activation through luciferase reporter assays (Fig. 4J). In summary, ERAdP interacts with Ubc13 to facilitate K63-linked ubiquitination of NEMO.

ERAdP potentiates the charging activity of Ubc13

Ubc13 was reported to be regulated by deubiquitylase A20 (29). A20 can target Ubc13 for K48-linked ubiquitination to mediate its proteasomal degradation, leading to downregulation of NF-κB pathway. We found that Ubc13 and TRAF6 were very stable after 24 h stimulation with PMA/IONO (Fig. 5A, 5B), and ERAdP silencing or overexpression did not alter the stability of Ubc13 and TRAF6. These data suggest that the regulation of Ubc13 stability is not involved in the ERAdP-induced NF-κB activation pathway.

We next established an in vitro ubiquitin charging assay to determine whether ERAdP influence the charging activity of

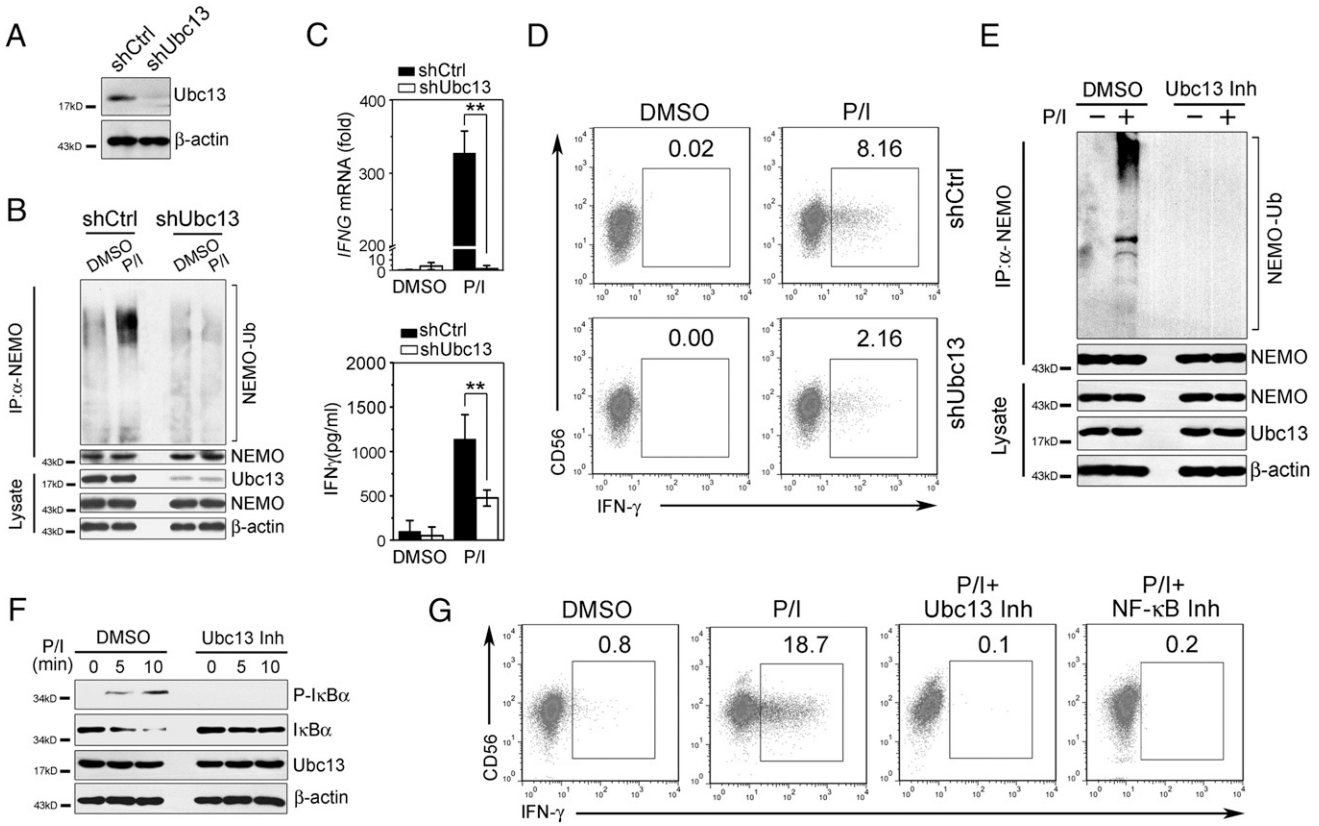

FIGURE 6. Ubc13 is required for ERAdP-induced IFN-γ production of NK cells. (**A**) Ubc13 is silenced in NKL cells. Ubc13 was knocked down and stably depleted NKL cell lines were established by puromycin selection. (**B**) Ubc13 silencing declines the ubiquitination of NEMO. Ubc13 silencing or scramble shRNA–treated (shCtrl) NKL cells were stimulated with PMA/IONO for 30 min. Cell lysates were precipitated with anti-NEMO Ab and subsequently immunoblotted with anti-ubiquitin Ab. (**C**) Ubc13 silencing reduces IFN-γ expression. Ubc13 silencing or shCtrl-treated NKL cells were stimulated with PMA/IONO for 6 h, followed by quantitative RT-PCR assays for *IFNG* mRNA (*upper panel*). Supernatants of NKL cells after 24 h treatment with PMA/IONO were analyzed by ELISA assays (*lower panel*). (**D**) Flow cytometry analysis of intracellular IFN-γ expression in Ubc13-depleted NKL cells after stimulation with PMA/IONO for 6 h. (**E**) The Ubc13 inhibitor can abolish the ubiquitination of NEMO. NKL cells were stimulated with PMA/IONO for 30 min with or without pretreatment of the Ubc13 inhibitor for 1 h. Lysates were immunoprecipitated with anti-NEMO Ab, followed by immunoblotting with anti-ubiquitin Ab. (**F**) The Ubc13 inhibitor disrupts the phosphorylation of IκBα with or without preincubation of the Ubc13 inhibitor. Ubc13-depleted NKL cells were stimulated with PMA/IONO for the indicated times, followed by immunoblotting. (**G**) Flow cytometry analysis of IFN-γ expression in NKL cells stimulated with PMA/IONO for 6 h with or without preincubation of the Ubc13 inhibitor or the NF-κB inhibitor. Data represent at least three separate experiments. $^{**}p < 0.01$.

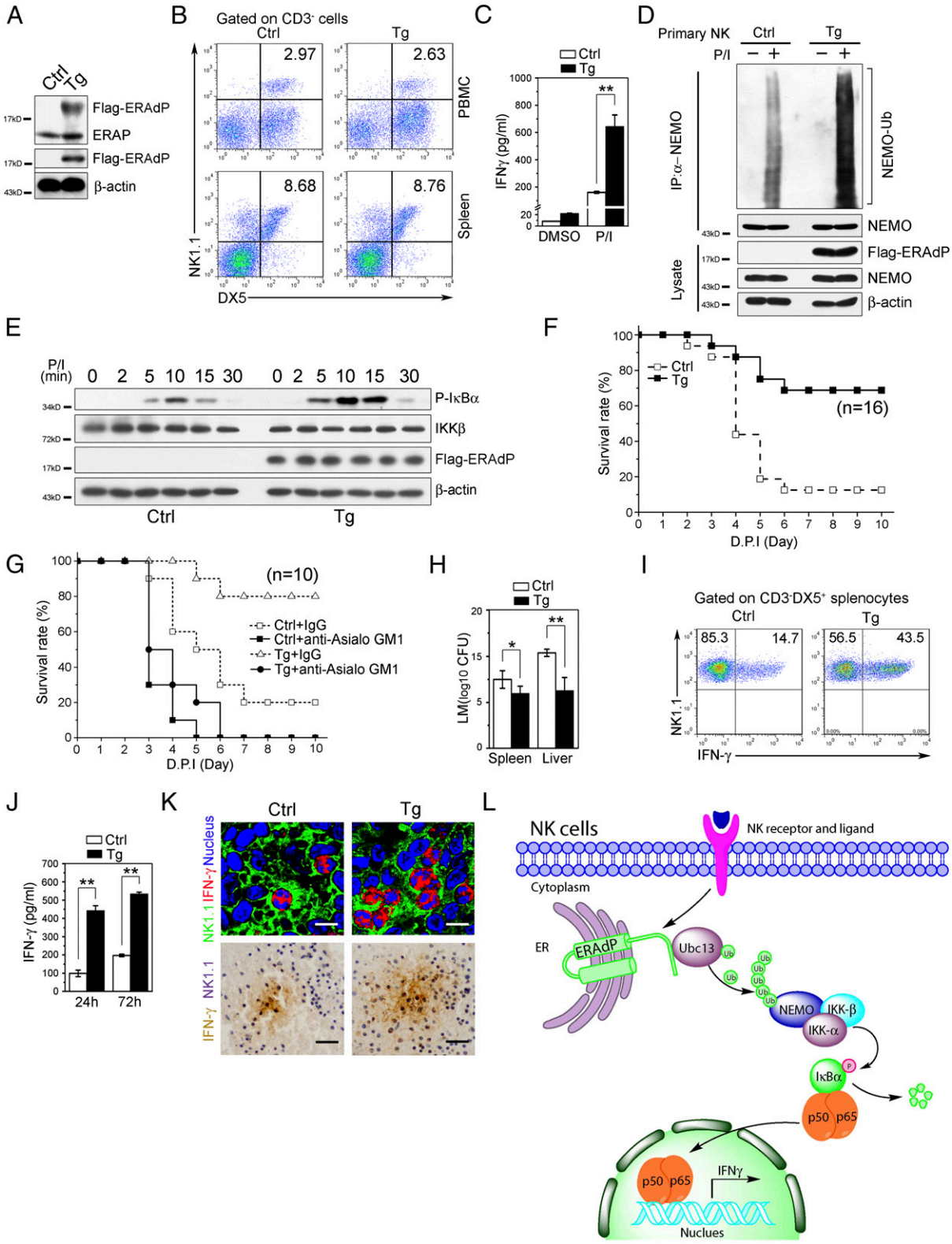

FIGURE 7. *ERAdP* Tg mice harbor hyperactivated NK cells that facilitate innate immune responses. (**A**) Flag-ERAdP is expressed in primary NK cells of *ERAdP* Tg mice. Primary NK cells were isolated from Flag-ERAdP-Tg (Tg) or Ctrl (WT littermates) mice spleens. Flag-ERAdP was detected by immunoblotting. (**B**) NK cell rates of ERAdP Tg mice are comparable to those of Ctrl mice. Mature NK cells ($CD3^-NK1.1^+DX5^+$) from PBMCs and spleens of Tg and Ctrl mice were analyzed by flow cytometry. (**C**) *ERAdP* Tg NK cells produce more IFN-γ. Primary NK cells isolated from Tg or Ctrl mice spleens were treated with PMA/IONO for 24 h. (**D**) *ERAdP* Tg NK cells generated more ubiquitination of NEMO with NK cell activation. Primary NK cells isolated from Tg or Ctrl mice spleens were stimulated with PMA/IONO for 30 min. The ubiquitination of NEMO was immunoprecipitated with anti-NEMO Ab and probed with anti-ubiquitin Ab. (**E**) *ERAdP* Tg NK cells produce more phosphorylation of IκBα. Primary NK cells isolated from Tg or Ctrl mice spleens were stimulated with PMA/IONO for the indicated times and detected by immunoblotting. (**F**) *ERAdP* Tg mice are resistant against *L. monocytogenes* infection. Survival curves were recorded for 10 d after Tg and Ctrl mice (n = 16/genotype) were i.p. injected with 2×10^6 *L. monocytogens*. (**G**) Depletion of NK cells in *ERAdP* Tg mice abolishes the resistance of *L. monocytogenes* infection. *ERAdP* Tg and Ctrl mice (*Figure legend continues*)

Ubc13. Intriguingly, we found that ERAdP significantly enhanced the charging activity of Ubc13 (Fig. 5C). Furthermore, ERAdP increased the Ubc13 charging activity in a dose-dependent manner (Fig. 5D). A chemical inhibitor (NSC697923) of Ubc13 was reported to inhibit the charging activity of Ubc13 and NF-κB activation (30). We found that the inhibitor NSC697923 completely abolished the ERAdP-augmented charging activity of Ubc13 (Fig. 5E). The Cys^{87} mutation abolishes enzymatic activity of Ubc13 (16). We observed that the inactive C87A-Ubc13 mutant abolished the charging activity of Ubc13 (Fig. 5F). Importantly, the C87A-Ubc13 mutant failed to catalyze NEMO ubiquitination through an in vitro reconstitution assay system (Fig. 5G). Moreover, the C87A-Ubc13 mutant abolished ERAdP-reinforced NEMO ubiquitination (Fig. 5G). These data indicate that the charging activity of Ubc13 is required for its enzymatic activity. Taken together, ERAdP acts as an activator to enhance Ubc13 charging activity.

Ubc13 is required for ERAdP-initiated IFN-γ production of NK cells

To examine whether Ubc13 is involved in NK cell activation, we silenced Ubc13 expression in NKL cells and established stable Ubc13-silenced NKL cell lines (Fig. 6A). Interestingly, Ubc13 depletion almost blocked NEMO ubiquitination with PMA/IONO stimulation (Fig. 6B). Additionally, Ubc13 silencing significantly declined IFN-γ production of NK cells (Fig. 6C), which is similar to ERAdP depletion. These results were verified by flow cytometry assays (Fig. 6D). Furthermore, the Ubc13 inhibitor NSC697923 completely blocked NEMO ubiquitination with PMA/IONO treatment in NK cells (Fig. 6E) or phosphorylation of IκBα (Fig. 6F). Accordingly, the Ubc13 inhibitor NSC697923 abolished IFN-γ production of NK cells (Fig. 6G). The NF-κB inhibitor disrupted IFN-γ production of NK cells as a positive Ctrl (Fig. 6G). These data suggest that Ubc13 is required for IFN-γ production in NK cells.

To further confirm that Ubc13 is required for ERAdP-mediated activation of NK cells, we silenced Ubc13 in ERAdP-overexpressing NKL cells (Supplemental Fig. 3A). Intriguingly, Ubc13 depletion remarkably impaired ERAdP-induced IFN-γ production (Supplemental Fig. 3B). Consistently, the Ubc13 inhibitor NSC697923 completely abolished the ERAdP-induced IFN-γ secretion (Supplemental Fig. 3C). In summary, Ubc13 is required for the ERAdP-induced IFN-γ secretion in NK cells.

ERAdP Tg mice harbor hyperactivated NK cells that facilitate NK cell–mediated immunity

To further explore the physiological function of ERAdP in vivo, we tried to generate *ERAdP* knockout mice. However, full deletion of *ERAdP* caused early embryonic lethality at embryonic day 6.5. Then we intended to establish *ERAdP* Flox mice for getting conditional knockout mice, but we failed after trying several strategies. Instead, we generated Flag-ERAdP Tg mice with a CD2 promoter–driven construct. Given that a Tg mouse model demonstrates overexpression of ERAdP in WT mice, we used the *ERAdP* Tg mice only to explore the relevantly physiological function of ERAdP in bacterial clearance. Flag-ERAdP was overexpressed in primary NK cells of *ERAdP* Tg mice (Fig. 7A). Absolute numbers of mature NK cells ($CD3^-NK1.1^+DX5^+$) in the periphery and spleen were similar in Tg mice compared with littermate Ctrl mice (Fig. 7B). However, Tg NK cells generated much more IFN-γ than did Ctrl NK cells with PMA/IONO stimulation (Fig. 7C). Moreover, Tg NK cells caused increased ubiquitination of NEMO (Fig. 7D) and concomitantly led to higher phosphorylation of IκBα (Fig. 7E), suggesting that *ERAdP* Tg NK cells reinforce IFN-γ production through the NF-κB activation pathway.

L. monocytogenes can effectively infect immunocompromised hosts (including humans and mice) mainly by contaminated food. NK cells contribute to the first defense against *L. monocytogenes* infection via IFN-γ secretion (9). Depletion of NK cells or IFN-γ resulted in severe exacerbation of *L. monocytogenes* infection and death in mice (31). We used the *L. monocytogenes* infection model to detect whether ERAdP-induced IFN-γ secretion exerted a critical role in the defense against *L. monocytogenes* infection. We i.p. infected mice with a lethal dose of *L. monocytogenes*. Fourteen of 16 littermate Ctrl mice died within 10 d (Fig. 7F), whereas only 5 Tg mice died until day 10. We depleted NK cells by i.p. injection of anti-Asialo GM1 mAb. We found that the resistance of Tg mice against *L. monocytogenes* infection was impaired upon depletion of NK cells (Fig. 7G), indicating that NK cells provided protection against *L. monocytogenes* infection.

To further confirm that IFN-γ plays a critical role in defense against *L. monocytogenes* infection, we infected mice with a sublethal dose of *L. monocytogenes*. As expected, Tg mice harbored a much lower *L. monocytogenes* load in spleens and livers than did Ctrl mice (Fig. 7H). Additionally, Tg mice had much more activated NK cells to generate IFN-γ in spleens after early *L. monocytogenes* infection compared with Ctrl mice (Fig. 7I). Accordingly, the IFN-γ level was much higher in Tg serum than in that of in Ctrl mice (Fig. 7J). Finally, through in situ histological staining, we observed more IFN-γ expression in splenic NK cells of Tg mice than that of Ctrl mice after *L. monocytogenes* infection (Fig. 7K). In summary, ERAdP-induced NK cell activation in Tg mice is more resistant to *L. monocytogenes* infection.

Discussion

NK cells play a pivotal role in the innate and adoptive immune responses through direct killing and cytokine secretion (2, 6). NK cell activation is controlled by a variety of activating and inhibitory receptors. However, the precise molecular mechanisms driving defined NK functions remain largely elusive. In this study, we identified a novel ER membrane protein, ERAdP, which is constitutively expressed in human and mouse NK cells. ERAdP is expressed at low levels in peripheral NKs of HBV-associated HCC patients, which is reminiscent of low expression of immune effector molecules such as perforin and granzyme H (5). We identified that ERAdP interacts with Ubc13 to potentiate its charging

($n = 10$/genotype) were i.p. injected with 2×10^6 *L. monocytogenes* after depletion of NK cells by anti–Asialo GM1 mAb. NK cell depletion was confirmed by FACS with anti-NK1.1 Ab staining. (**H**) Tg and Ctrl mice were i.p. infected with a sublethal dose of *L. monocytogenes* (3×10^5). After 3 d, spleens and livers were homogenized with PBS and the supernatants were analyzed for bacterial load. (**I**) Flow cytometry analysis of IFN-γ production in NK cells ($CD3^-DX5^+NK1.1^+IFN\text{-}\gamma^+$ cells) in the spleens from Tg and Ctrl mice at 24 h after 3×10^5 *L. monocytogenes* i.p. infection. (**J**) Serum IFN-γ of Tg and Ctrl mice was detected by ELISA assays 3 d after 3×10^5 *L. monocytogenes* i.p. infection. (**K**) Immunofluorescence staining of IFN-γ (red) and NK1.1 (green) (*upper panel*), as well as immunohistochemistry staining of IFN-γ (*lower panel*) in paraffin sections of spleens from Tg and Ctrl mice at 24 h after *L. monocytogenes* infection. Scale bars: *upper panel*, 5 μm; *lower panel*, 50 μm. Data are representative of at least three independent experiments and are shown as means ± SD. (**L**) A working model for the regulation of IFN-γ production by ERAdP in NK cells through Ubc13-mediated NF-κB activation. $^*p < 0.05$, $^{**}p < 0.01$.

activity (Fig. 7L). Thus, ERAdP augments Ubc13-mediated NEMO ubiquitination to trigger the Ubc13-mediated NF-κB pathway, leading to NK cell activation. Importantly, *ERAdP* Tg mice have hyperactivated NK cells that are more resistant to infections.

Bcl10, a caspase recruitment domain (CARD) protein, associates with Malt1 adaptor protein as a major regulator of TCR- and BCR-mediated NF-κB activation (32, 33). Carma1 (also termed CARD11 and Bimp3) interacts with Bcl10 through CARD–CARD interaction. These three proteins form the CBM complex (34, 35). Ligand engagement first activates the receptor-associated Src kinases to mediate phosphorylation of Carma1. Carma1 phosphorylation initiates the CBM complex assembly, which recruits the ubiquitination machine E3 (TRAF6)/E2 (Ubc13) complex and the IKK complex (13). The ubiquitination of NEMO and phosphorylation of IKKα/β lead to full activation of the IKK complex and subsequent NF-κB activation. Hara et al. (36) reported that Carma1 or Bcl10 deficiency abolishes cytokine/chemokine production of NK cells owing to impaired NF-κB activation, suggesting that the CBM complex may play an important role in NK cell activation. In this study we observed that ERAdP did not affect the assembly of the CBM complex, but it facilitated the NEMO ubiquitination by promoting the charging activity of Ubc13. Moreover, ERAdP could positively induce cytokine production of NK cells, which is reminiscent of the CBM complex–mediated NF-κB activation pathway (37, 38).

Ubc13 has been reported to be regulated by deubiquitylase A20, OTUB1, and the *Shigella flexneri* effector OspI (29, 39, 40). A20, together with TAX1BP1, interacts with Ubc13 and UbcH5c, resulting in its ubiquitination for degradation, which downregulates NF-κB activation (29). OTUB1 directly binds to and inhibits Ubc13 to suppress double-stranded break–induced histone ubiquitination, independent of its deubiquitylase activity (40). The interaction of OTUB1 and Ubc13 positions the N-terminal helix of OTUB1 to interfere with Uev1a binding to Ubc13 and the subsequent attack on the thioester bond by the Uev1a-linked acceptor ubiquitin. Recently, OspI was reported to suppress the TRAF6-mediated signaling pathway and restrain acute inflammatory responses against bacterial infection (39). OspI is a glutamine deamidase and deamidates the residue Glu^{100} of Ubc13 to form a glutamic acid residue. This modification abolishes the ubiquitin charging activity of Ubc13, leading to inactivation of the NF-κB pathway. In this study, we showed that ERAdP directly binds to Ubc13 and potentiates its charging activity as a positive regulator.

ERAdP robustly interacts with Ubc13 after NK cell activation upon PMA/IONO stimulation or crosslinking with activating receptors. Actually, ERAdP was observed to bind Bcl10 after NK cell activation (data not shown). Given that the CBM complex was reported to recruit TRAF6/Ubc13 complex, it is possible that the assembled CBM complex in activated NK cells acts as a scaffold to mediate ERAdP–Ubc13 interaction. This phenomenon needs further investigation.

Secretion of soluble cytokines by NK cells in early innate immune responses significantly impacts the recruitment and function of other hematopoietic cells to exert their physiological roles. Besides promoting IFN-γ production, ERAdP could induce secretion of other cytokines such as TNF-α and GM-CSF (data not shown). IFN-γ is mainly produced by NK cells at early stages of a variety of immune responses (41, 42). IFN-γ can act directly on $CD8^+$ T cells to increase their numbers upon viral infection (43). We previously showed that IFN-γ produced by NK cells exerts a crucial role for the priming of CTL responses for tumor rejection (6). Many studies showed that NK cells and secreted IFN-γ are implicated in the resistance against several infectious diseases, including CMV, HIV, *Mycobacterium tuberculosis, L. monocytogenes*, and hepatitis virus (9–11). In this study, we showed that *ERAdP* Tg mice augment NK cell activation and IFN-γ generation that exert a critical role in the eradication of intracellular pathogens such as *L. monocytogenes*. We are still investigating the ERAdP-induced eradication of virus infection. Therefore, understanding the mechanism of ERAdP-mediated NK cell activation will provide strategies to treat infectious diseases for future clinical implications.

Acknowledgments

We thank Dr. André Veillette for providing the CD2 promotor–driven Tg vector and Dr. Jiyong Zhao for providing the Ubc13 inhibitor. We thank Drs. Honglian Zhang, Haidong Tang, Li Wang, Lianfeng Wu, Lei Shi, and Deqing Hu for helpful discussion. We also thank Junying Jia, Chunchun Liu, and Peng Xue for technical assistance.

Disclosures

The authors have no financial conflicts of interest.

References

1. Lanier, L. L. 2005. NK cell recognition. *Annu. Rev. Immunol.* 23: 225–274.
2. Long, E. O., H. S. Kim, D. Liu, M. E. Peterson, and S. Rajagopalan. 2013. Controlling natural killer cell responses: integration of signals for activation and inhibition. *Annu. Rev. Immunol.* 31: 227–258.
3. Vivier, E., E. Tomasello, M. Baratin, T. Walzer, and S. Ugolini. 2008. Functions of natural killer cells. *Nat. Immunol.* 9: 503–510.
4. Zhong, C., C. Li, X. Wang, T. Toyoda, G. Gao, and Z. Fan. 2012. Granzyme K inhibits replication of influenza virus through cleaving the nuclear transport complex importin α1/β dimer of infected host cells. *Cell Death Differ.* 19: 882–890.
5. Tang, H., C. Li, L. Wang, H. Zhang, and Z. Fan. 2012. Granzyme H of cytotoxic lymphocytes is required for clearance of the hepatitis B virus through cleavage of the hepatitis B virus X protein. *J. Immunol.* 188: 824–831.
6. Fan, Z., P. Yu, Y. Wang, Y. Wang, M. L. Fu, W. Liu, Y. Sun, and Y.-X. Fu. 2006. NK-cell activation by LIGHT triggers tumor-specific $CD8^+$ T-cell immunity to reject established tumors. *Blood* 107: 1342–1351.
7. Lanier, L. L. 2008. Up on the tightrope: natural killer cell activation and inhibition. *Nat. Immunol.* 9: 495–502.
8. Liu, S., H. Zhang, M. Li, D. Hu, C. Li, B. Ge, B. Jin, and Z. Fan. 2013. Recruitment of Grb2 and SHIP1 by the ITT-like motif of TIGIT suppresses granule polarization and cytotoxicity of NK cells. *Cell Death Differ.* 20: 456–464.
9. Pamer, E. G. 2004. Immune responses to *Listeria monocytogenes*. *Nat. Rev. Immunol.* 4: 812–823.
10. Lanier, L. L. 2008. Evolutionary struggles between NK cells and viruses. *Nat. Rev. Immunol.* 8: 259–268.
11. Browne, S. K., P. D. Burbelo, P. Chetchotisakd, Y. Suputtamongkol, S. Kiertiburanakul, P. A. Shaw, J. L. Kirk, K. Jutivorakool, R. Zaman, L. Ding, et al. 2012. Adult-onset immunodeficiency in Thailand and Taiwan. *N. Engl. J. Med.* 367: 725–734.
12. Sen, R. 2011. The origins of NF-κB. *Nat. Immunol.* 12: 686–688.
13. Wu, C. J., and J. D. Ashwell. 2008. NEMO recognition of ubiquitinated Bcl10 is required for T cell receptor-mediated NF-κB activation. *Proc. Natl. Acad. Sci. USA* 105: 3023–3028.
14. Shambharkar, P. B., M. Blonska, B. P. Pappu, H. Li, Y. You, H. Sakurai, B. G. Darnay, H. Hara, J. Penninger, and X. Lin. 2007. Phosphorylation and ubiquitination of the IκB kinase complex by two distinct signaling pathways. *EMBO J.* 26: 1794–1805.
15. Sun, L., L. Deng, C. K. Ea, Z. P. Xia, and Z. J. Chen. 2004. The TRAF6 ubiquitin ligase and TAK1 kinase mediate IKK activation by BCL10 and MALT1 in T lymphocytes. *Mol. Cell* 14: 289–301.
16. Deng, L., C. Wang, E. Spencer, L. Yang, A. Braun, J. You, C. Slaughter, C. Pickart, and Z. J. Chen. 2000. Activation of the IκB kinase complex by TRAF6 requires a dimeric ubiquitin-conjugating enzyme complex and a unique polyubiquitin chain. *Cell* 103: 351–361.
17. Zhou, H., I. Wertz, K. O'Rourke, M. Ultsch, S. Seshagiri, M. Eby, W. Xiao, and V. M. Dixit. 2004. Bcl10 activates the NF-κB pathway through ubiquitination of NEMO. *Nature* 427: 167–171.
18. Yin, Q., S. C. Lin, B. Lamothe, M. Lu, Y. C. Lo, G. Hura, L. Zheng, R. L. Rich, A. D. Campos, D. G. Myszka, et al. 2009. E2 interaction and dimerization in the crystal structure of TRAF6. *Nat. Struct. Mol. Biol.* 16: 658–666.
19. Yamamoto, M., S. Sato, T. Saitoh, H. Sakurai, S. Uematsu, T. Kawai, K. J. Ishii, O. Takeuchi, and S. Akira. 2006. Cutting edge: pivotal function of Ubc13 in thymocyte TCR signaling. *J. Immunol.* 177: 7520–7524.
20. Andersen, P. L., H. Zhou, L. Pastushok, T. Moraes, S. McKenna, B. Ziola, M. J. Ellison, V. M. Dixit, and W. Xiao. 2005. Distinct regulation of Ubc13 functions by the two ubiquitin-conjugating enzyme variants Mms2 and Uev1A. *J. Cell Biol.* 170: 745–755.
21. Moraes, T. F., R. A. Edwards, S. McKenna, L. Pastushok, W. Xiao, J. N. Glover, and M. J. Ellison. 2001. Crystal structure of the human ubiquitin conjugating enzyme complex, hMms2-hUbc13. *Nat. Struct. Biol.* 8: 669–673.
22. Ye, Y., and M. Rape. 2009. Building ubiquitin chains: E2 enzymes at work. *Nat. Rev. Mol. Cell Biol.* 10: 755–764.

23. VanDemark, A. P., R. M. Hofmann, C. Tsui, C. M. Pickart, and C. Wolberger. 2001. Molecular insights into polyubiquitin chain assembly: crystal structure of the Mms2/Ubc13 heterodimer. *Cell* 105: 711–720.
24. Eddins, M. J., C. M. Carlile, K. M. Gomez, C. M. Pickart, and C. Wolberger. 2006. Mms2-Ubc13 covalently bound to ubiquitin reveals the structural basis of linkage-specific polyubiquitin chain formation. *Nat. Struct. Mol. Biol.* 13: 915–920.
25. Kim, H. S., A. Das, C. C. Gross, Y. T. Bryceson, and E. O. Long. 2010. Synergistic signals for natural cytotoxicity are required to overcome inhibition by c-Cbl ubiquitin ligase. *Immunity* 32: 175–186.
26. Xia, P., S. Wang, Y. Du, Z. Zhao, L. Shi, L. Sun, G. Huang, B. Ye, C. Li, Z. Dai, et al. 2013. WASH inhibits autophagy through suppression of Beclin 1 ubiquitination. *EMBO J.* 32: 2685–2696.
27. Guo, Y., J. Chen, L. Shi, and Z. Fan. 2010. Valosin-containing protein cleavage by granzyme K accelerates an endoplasmic reticulum stress leading to caspase-independent cytotoxicity of target tumor cells. *J. Immunol.* 185: 5348–5359.
28. Sun, W., Y. Li, L. Chen, H. Chen, F. You, X. Zhou, Y. Zhou, Z. Zhai, D. Chen, and Z. Jiang. 2009. ERIS, an endoplasmic reticulum IFN stimulator, activates innate immune signaling through dimerization. *Proc. Natl. Acad. Sci. USA* 106: 8653–8658.
29. Shembade, N., A. Ma, and E. W. Harhaj. 2010. Inhibition of NF-κB signaling by A20 through disruption of ubiquitin enzyme complexes. *Science* 327: 1135–1139.
30. Pulvino, M., Y. Liang, D. Oleksyn, M. DeRan, E. Van Pelt, J. Shapiro, I. Sanz, L. Chen, and J. Zhao. 2012. Inhibition of proliferation and survival of diffuse large B-cell lymphoma cells by a small-molecule inhibitor of the ubiquitin-conjugating enzyme Ubc13-Uev1A. *Blood* 120: 1668–1677.
31. Dunn, P. L., and R. J. North. 1991. Early gamma interferon production by natural killer cells is important in defense against murine listeriosis. *Infect. Immun.* 59: 2892–2900.
32. Ruefli-Brasse, A. A., D. M. French, and V. M. Dixit. 2003. Regulation of NF-κB-dependent lymphocyte activation and development by paracaspase. *Science* 302: 1581–1584.
33. Ruland, J., G. S. Duncan, A. Wakeham, and T. W. Mak. 2003. Differential requirement for Malt1 in T and B cell antigen receptor signaling. *Immunity* 19: 749–758.
34. Shinohara, H., S. Maeda, H. Watarai, and T. Kurosaki. 2007. IκB kinase β-induced phosphorylation of CARMA1 contributes to CARMA1 Bcl10 MALT1 complex formation in B cells. *J. Exp. Med.* 204: 3285–3293.
35. Qiao, Q., C. Yang, C. Zheng, L. Fontán, L. David, X. Yu, C. Bracken, M. Rosen, A. Melnick, E. H. Egelman, and H. Wu. 2013. Structural architecture of the CARMA1/Bcl10/MALT1 signalosome: nucleation-induced filamentous assembly. *Mol. Cell* 51: 766–779.
36. Hara, H., C. Ishihara, A. Takeuchi, L. Xue, S. W. Morris, J. M. Penninger, H. Yoshida, and T. Saito. 2008. Cell type-specific regulation of ITAM-mediated NF-κB activation by the adaptors, CARMA1 and CARD9. *J. Immunol.* 181: 918–930.
37. Gross, O., C. Grupp, C. Steinberg, S. Zimmermann, D. Strasser, N. Hannesschläger, W. Reindl, H. Jonsson, H. Huo, D. R. Littman, et al. 2008. Multiple ITAM-coupled NK-cell receptors engage the Bcl10/Malt1 complex via Carma1 for NF-κB and MAPK activation to selectively control cytokine production. *Blood* 112: 2421–2428.
38. Malarkannan, S., J. Regunathan, H. Chu, S. Kutlesa, Y. Chen, H. Zeng, R. Wen, and D. Wang. 2007. Bcl10 plays a divergent role in NK cell-mediated cytotoxicity and cytokine generation. *J. Immunol.* 179: 3752–3762.
39. Sanada, T., M. Kim, H. Mimuro, M. Suzuki, M. Ogawa, A. Oyama, H. Ashida, T. Kobayashi, T. Koyama, S. Nagai, et al. 2012. The *Shigella flexneri* effector OspI deamidates UBC13 to dampen the inflammatory response. *Nature* 483: 623–626.
40. Nakada, S., I. Tai, S. Panier, A. Al-Hakim, S. Iemura, Y.-C. Juang, L. O'Donnell, A. Kumakubo, M. Munro, F. Sicheri, et al. 2010. Non-canonical inhibition of DNA damage-dependent ubiquitination by OTUB1. *Nature* 466: 941–946.
41. Martín-Fontecha, A., L. L. Thomsen, S. Brett, C. Gerard, M. Lipp, A. Lanzavecchia, and F. Sallusto. 2004. Induced recruitment of NK cells to lymph nodes provides IFN-γ for T_H1 priming. *Nat. Immunol.* 5: 1260–1265.
42. Fauriat, C., E. O. Long, H. G. Ljunggren, and Y. T. Bryceson. 2010. Regulation of human NK-cell cytokine and chemokine production by target cell recognition. *Blood* 115: 2167–2176.
43. Whitmire, J. K., J. T. Tan, and J. L. Whitton. 2005. Interferon-γ acts directly on $CD8^+$ T cells to increase their abundance during virus infection. *J. Exp. Med.* 201: 1053–1059.